Published in final edited form as:
J Neurosci Res. 2012 February ; 90(2): 346–355. doi:10.1002/jnr.22757.

Regional Brain Axial and Radial Diffusivity Changes During Development

Rajesh Kumar[1], **Haidang D. Nguyen**[1], **Paul M. Macey**[2,3], **Mary A. Woo**[2], and **Ronald M. Harper**[1,3,*]

[1]Department of Neurobiology, David Geffen School of Medicine at UCLA, University of California at Los Angeles, Los Angeles, CA 90095-1763, USA

[2]School of Nursing, University of California at Los Angeles, Los Angeles, CA 90095-1702, USA

[3]Brain Research Institute, University of California at Los Angeles, Los Angeles, CA 90095-1761, USA

Abstract

The developing human brain shows rapid myelination and axonal changes during childhood, adolescence and early adulthood, requiring successive evaluations to determine normative values for potential pathological assessment. Fiber characteristics can be examined by axial and radial diffusivity procedures, which measure water diffusion parallel and perpendicular to axons, and primarily show axonal status and myelin changes, respectively. Such measures are lacking from wide-spread sites for the developing brain. Diffusion tensor imaging data were acquired from 30 healthy subjects (age, 17.7±4.6, range 8–24 years; body-mass-index, 21.5±4.5 kg/m^2; 18 male) using a 3.0-Tesla MRI scanner. Diffusion tensors were calculated, principal eigenvalues determined, and axial and radial diffusivity maps calculated and normalized to a common space. A set of regions-of-interest were outlined from wide-spread brain areas within rostral, thalamic, hypothalamic, cerebellar, and pontine regions, and average diffusivity values were calculated using normalized diffusivity maps and these regions-of-interest masks. Age-related changes were assessed with Pearson's correlations, and gender differences evaluated with Student's t-tests. Axial and radial diffusivity values declined with age in the majority of brain areas, except for mid hippocampus, where axial diffusivity values correlated positively with age. Gender differences emerged within putamen, thalamic, hypothalamic, cerebellar, limbic, temporal, and other cortical sites. Documentation of normal axial and radial diffusivity values will help assess disease-related tissue changes. Axial and radial diffusivity change with age, with fiber structure and organization differing between sexes in several brain areas. The findings may underlie gender-based functional characteristics, and mandate partitioning age- and gender-related changes during developmental brain pathology evaluation.

Keywords

Diffusion tensor imaging; Axons; Myelin; Brain maturation; Water diffusion

[*]**Corresponding Author:** Ronald M. Harper, Ph.D., Department of Neurobiology, David Geffen School of Medicine at UCLA, University of California at Los Angeles, Los Angeles, CA 90095-1763, USA, Tel: 310-825-5303; Fax: 310-825-2224, rharper@ucla.edu.

Introduction

The developing human brain shows rapid changes in axonal characteristics with age, including axonal density, caliber, and myelin (Barnea-Goraly et al. 2005; Mukherjee et al. 2002). Disease-related pathological processes induce alterations in axonal integrity, including axonal and myelin loss (DeLuca et al. 2006; Kumar et al. 2008; Kumar et al. 2010; Mitchell et al. 2003; Trapp et al. 1998). Pathological axonal changes can be evaluated effectively after controlling for age-related variations in axonal characteristics. However, description of normal age-related axonal characteristics from wide-spread sites is lacking for the developing brain.

Such normative age-related tissue changes can be determined by axial and radial diffusivity procedures. Axial diffusivity measures diffusion of water parallel to axons, and primarily shows axonal status, and radial diffusivity measures water diffusion perpendicular to fibers, and mainly indicates myelin changes (Song et al. 2002; Song et al. 2005). Axial diffusivity values increase in areas with reduced axonal density or caliber, and radial diffusivity values increase with loss of myelin integrity in chronic pathological conditions (Della Nave et al. 2010; Hasan et al. 2008; Kumar et al. 2008; Kumar et al. 2010). However, axial and radial diffusivity values decrease with increased corresponding axonal density or caliber, and myelin increases with age in the developing brain (Mukherjee et al. 2002; Qiu et al. 2008; Suzuki et al. 2003). Thus, axial and radial diffusivity measures can help determine changes in fiber characteristics with age in healthy subjects during childhood, adolescence and young adulthood. Since females differ significantly in cerebral blood flow over males (Jones et al. 1998), and blood perfusion characteristics may significantly alter the course of pathological or progressive changes, any evaluation of axonal characteristics must include the contribution of gender.

Our aim was to assess normal age-related changes in axial and radial diffusivity in wide-spread brain areas, and determine sex-related differences in those brain sites in healthy subjects from childhood, adolescents and young adults.

Materials and Methods

Subjects

We studied 30 healthy subjects (Male, 18, mean age ± SD = 18.5±4.6 years, age range = 10–24 years, mean body-mass-index ±SD = 22.2±4.9 kg/m^2; Female, 12, mean age ± SD = 16.5±4.6 years, age range = 8–22 years, mean body-mass-index ±SD = 20.5±3.7 kg/m^2). All subjects had participated in previously-published pediatric studies of issues unrelated to the current interest (Kumar et al. 2010; Ogren et al. 2010); thus, male and female subjects were not age-matched, but were of the same age-range. Subjects were recruited through advertisements at the university campus and from the neighboring community. We excluded all subjects with conditions that might affect brain tissue, brain images, or might not be safe for subjects in a high-magnetic field environment, as outlined in the web-site of the Institute for Magnetic Resonance Safety, Education, and Research (http://www.mrisafety.com/).

All subjects and their parents/guardians gave informed written consent/assent prior to the study, and the study protocol was approved by the Institutional Review Board of the University of California at Los Angeles. Personal identifiable information was removed from the records after completion of the analyses.

Magnetic resonance imaging

We performed all brain imaging studies using a 3.0-Tesla magnetic resonance imaging (MRI) scanner (Magnetom Tim-Trio; Siemens, Erlangen, Germany). We used a receive-

only 8-channel phased-array head-coil and a whole-body transmitter coil for MRI studies. Foam pads on both sides of the head were used to reduce head motion during MRI. High-resolution T1-weighted images were collected using a magnetization prepared rapid acquisition gradient-echo (MPRAGE) pulse sequence [repetition-time (TR) = 2200 ms; echo-time (TE) = 2.34 ms; inversion time = 900 ms; flip angle (FA) = 9°; matrix size = 320×320; field-of-view (FOV) = 230×230 mm; slice thickness = 0.9 mm; slices = 192]. Proton-density (PD) and T2-weighted images were acquired, covering the whole brain, using a dual-echo turbo spin-echo pulse sequence (TR = 10,000 ms; TE1, 2 = 12, 119 ms; FA = 130°; matrix size = 256×256; FOV = 230×230 mm; slice thickness = 3.5 mm; turbo factor = 5). Diffusion tensor imaging (DTI) data were collected using a single-shot echo-planar-imaging with twice-refocused spin-echo pulse sequence (TR = 10,000 ms; TE = 87 ms; FA = 90°; readout bandwidth = 1346 Hz/pixel; matrix size = 128×128; FOV = 230×230 mm; slice thickness = 2.0 mm; no interslice-gap; diffusion gradient directions = 64; b = 0 and 700 s/mm^2). The generalized autocalibrating partially parallel acquisition (GRAPPA) parallel imaging technique, with an acceleration factor of two, was used to collect DTI data, and two DTI series were collected individually with the same imaging parameters for subsequent averaging.

Data processing

We used the statistical parametric mapping package SPM8 (http://www.fil.ion.ucl.ac.uk/spm/), DTI-Studio (v 3.0.1, https://www.mristudio.org/) (Jiang et al. 2006), MRIcroN (Rorden et al. 2007), and MATLAB-based (The MathWorks Inc., Natick, MA) custom software for data processing. Proton-density-, T2-, and T1-weighted images were examined visually to ensure no serious anatomical defects were apparent, including cysts, tumors, or any other lesions before data processing. No subjects showed any of these abnormalities on visual examination of brain images. Non-diffusion and diffusion-weighted data were also evaluated for motion and other imaging artifacts to ensure that images were acceptable for subsequent analysis.

Calculation of axial and radial diffusivity indices

The average background noise value outside the brain areas was calculated by assessing absolute signal intensity levels on non-diffusion and diffusion-weighted images, and this value was used to exclude non-brain regions during axial and radial diffusivity calculation, as described earlier (Kumar et al. 2008; Kumar et al. 2010; Kumar et al. 2011b). Using diffusion-weighted images (b = 700 s/mm^2), collected from 64 diffusion directions, and non-diffusion images (b = 0 s/mm^2), diffusion tensor matrices were calculated with DTI-Studio software (Jiang et al. 2006). The diffusion tensor matrices were diagonalized at each voxel, and three principal eigenvalues ($\lambda1$, $\lambda2$, and $\lambda3$) were derived (Basser and Pierpaoli 1998; Pierpaoli and Basser 1996). Using principal eigenvalues, we calculated axial ($\lambda_{\parallel} = \lambda1$) and radial [$\lambda_{\perp} = (\lambda2 + \lambda3)/2$] diffusivity maps from each DTI series (Kumar et al. 2008; Kumar et al. 2010; Kumar et al. 2011b; Song et al. 2002; Song et al. 2005).

Realignment, averaging, and normalization

We realigned both axial and radial diffusivity maps, derived from two DTI series of each subject; these maps were averaged to create one axial and one radial diffusivity map for each subject (Kumar et al. 2008; Kumar et al. 2010; Kumar et al. 2011b). Both b0 images (non-diffusion weighted images), derived from both series, were also realigned, and averaged. The averaged axial and radial diffusivity maps were used for subsequent analyses, and b0 images were used for normalization and background purposes.

Both averaged axial and radial diffusivity maps were normalized to Montreal Neurological Institute (MNI) space. Using *a priori*-defined distributions of gray, white, and cerebrospinal

fluid (CSF) tissue types (Ashburner and Friston 2005), b0 images of each subject were normalized to the MNI space template, and the resulting normalization parameters were used to normalize corresponding axial and radial diffusivity maps. The normalized b0 images of all subjects were averaged to create mean background images, which were used to outline regions-of-interest (ROIs) for further analysis.

Region of interest analyses

A set of rectangular ROIs from multiple brain sites were created using mean background images derived from normalized b0 images of all subjects with MRIcroN software. These ROIs were included from multiple brain areas of rostral, thalamic and hypothalamic, pontine, and cerebellar regions (Fig. 1). All ROIs included three consecutive brain slices, and the size of the ROI was selected to fit within the examined structure. Brain sites that were very close to CSF, such as medullary regions, were excluded for evaluation, since small mis-registrations of axial and radial diffusivity maps to MNI space may contaminate axial and radial diffusivity values of those areas.

Rostral brain areas

Regions assessed within the rostral brain included cortical gray and white matter, amygdala, basal ganglia, and hippocampus. Bilateral structures, including the anterior, mid, and posterior cingulate and insular cortices, caudate nuclei, putamen, globus pallidus, frontal white and gray matter, amygdala, ventral, mid, and dorsal hippocampus and temporal white matter, midline occipital gray matter, and occipital white matter, were assessed. Other unilateral sites, including the anterior, mid, and posterior corpus callosum, were also examined.

Thalamic and hypothalamic regions

Both thalamic and hypothalamic areas were examined. The ROIs were outlined within the left and right hypothalamic regions and thalamic areas, including anterior, mid, and posterior portions of those structures.

Pontine and cerebellar structures

Unilateral and bilateral ROIs were outlined within the pons and cerebellum. Unilateral ROIs were delineated within the ventral, mid, and caudal pons, and cerebellar deep nuclei, and bilateral ROIs were created within the caudal and rostral cerebellar cortices, and inferior, mid, and superior cerebellar peduncles.

Mean axial and radial diffusivity calculation

Mean axial and radial diffusivity values of different brain sites were determined using ROI brain masks of those areas and normalized axial and radial diffusivity maps, as described previously with different data (Kumar et al. 2011a). Axial and radial diffusivity values of the different brain sites were assessed for age-related changes; values of these sites were also compared between genders to determine male-female differences.

Statistical analyses

The Statistical Package for the Social Sciences (SPSS V 18.0, Chicago, IL, USA) software was used for statistical evaluation of data. We used Pearson's correlation procedures to examine relationships between combined male and female axial and radial diffusivity values of different brain regions with age. Male-female differences in axial and radial diffusivity values in those regions were evaluated with Student's t-tests. A p value less than 0.05 was considered statistically significant.

Results

The range of age for all subjects was 8–24 years. No significant differences in age appeared between the male and female groups (males vs. females; 18.5±4.6 vs. 16.5±4.6 years, p = 0.25). Body mass index values of males were also equivalent to females (males vs. females; 22.2±4.9 vs. 20.5±3.7 kg/m^2, p = 0.31).

Rostral brain areas

Brain sites within the rostral brain that showed, based on the combined male and female data, decreased and increased axial diffusivity values and decreased radial diffusivity values with age are shown in scatter plots (Figs. 2, 3). Relationships between male and female values with age are also displayed in those plots, but only for those sites that showed significant relationships between combined data and age (Figs. 2, 3). Bilateral structures, based on combined male and female data, including the caudate nuclei (left, r = − 0.46, p = 0.01; right, r = − 0.50, p = 0.005) and frontal white matter (left, r = − 0.58, p = 0.001; right, r = − 0.54, p = 0.002), showed negative relationships between axial diffusivity and age; caudate nuclei (left, r = − 0.56, p = 0.001; right, r = − 0.50, p = 0.005), putamen (left, r = − 0.72, p < 0.001; right, r = − 0.62, p < 0.001), mid cingulated (left, r = − 0.38, p = 0.04; right, r = − 0.39, p = 0.03), and globus pallidus (left, r = − 0.50, p = 0.005; right, r = − 0.37, p = 0.04) also showed inverse correlations between radial diffusivity values and age. Other unilateral brain sites that showed negative correlations between axial diffusivity and age in combined male and female data included anterior (r = − 0.53, p = 0.003) and posterior (r = − 0.37, p = 0.04) corpus callosum, left globus pallidus (r = − 0.37, p = 0.04), and right ventral (r = − 0.53, p = 0.002) and left mid (r = − 0.42, p = 0.02) and dorsal (r = − 0.39, p = 0.03) temporal white matter, while positive correlations between axial diffusivity and age included the right mid hippocampus (r = 0.41, p = 0.02). Unilateral brain areas showing negative correlations between radial diffusivity in combined male and female data and age included the left anterior insula (r = − 0.42, p = 0.02), right frontal (r = − 0.40, p = 0.03), and mid (r = − 0.49, p = 0.006) and dorsal temporal (r = − 0.43, p = 0.02) white matter.

Thalamic and hypothalamic regions

Multiple brain sites within thalamic areas showed decreased axial and radial diffusivity values in combined data with age (Fig. 4). Brain sites that showed inverse relationships between axial diffusivity in combined data and age included the left anterior (r = − 0.49, p = 0.006) and right mid (r = − 0.44, p = 0.01) and posterior (r = − 0.44, p = 0.01) thalamus, and between radial diffusivity and age included the bilateral mid thalamus (left, r = − 0.52, p = 0.004; right, r = − 0.56, p = 0.001).

Pontine and cerebellar structures

The mid pons (r = − 0.49, p = 0.006) and bilateral mid cerebellar peduncles (left, r = − 0.44, p = 0.01; right, r = − 0.44, p = 0.02) showed negative correlations between axial diffusivity in combined data and age (Fig. 4). The mid pons (r = − 0.44, p = 0.01) and right rostral cerebellar cortex (r = − 0.49, p = 0.006) showed inverse relationships between radial diffusivity values in combined data and age (Fig. 4).

Male-female differences

Multiple brain regions showed axial and radial diffusivity differences between sexes (Table 1–3). Brain areas that showed axial diffusivity differences between males and females included the left putamen (p = 0.002), left mid temporal white matter (p = 0.02), left amygdala (p = 0.02), and right mid cerebellar peduncles (p = 0.007). Radial diffusivity differences between genders emerged in the left ventral hippocampus (p = 0.03), left

amygdala (p = 0.02), right midline occipital gray matter (p = 0.03), left mid thalamus (p = 0.04), right mid cingulate (0.02), right hypothalamus (p = 0.02), and right rostral cerebellar cortex (p = 0.04).

Discussion

Overview

Multiple brain sites in developing subjects showed negative relationships between axial and radial diffusivity values and age, except for the mid hippocampus where axial diffusivity was positively correlated with age. Gender differences emerged in multiple brain areas, including the basal ganglia, portions of the limbic system, temporal and occipital lobes, thalamus and hypothalamus, and cerebellar sites. Normative axial and radial diffusivity values from regions across the brain will assist comparisons with disease-related tissue changes. Male-female differences and age-related changes in axial and radial diffusivity values in several brain sites suggest the need for controlling these confounds during any evaluation for pathology.

Diffusion tensor imaging and tissue characteristics

Diffusion tensor imaging assesses diffusion of water molecules within the tissue and evaluates tissue changes. The procedure has been used to examine brain tissue changes in developmental studies (Mukherjee and McKinstry 2006; Neil et al. 1998), neurodegenerative diseases, including myelin-related diseases such as Krabbe disease (Guo et al. 2001), dementia (Larsson et al. 2004), and multiple sclerosis (Filippi et al. 2001), and various neurological conditions, including stroke (Werring et al. 2000), and traumatic brain injury (Huisman et al. 2004). The procedure primarily evaluates myelin and axonal characteristics; however, other aspects of fiber characteristics, such as orientation coherence, number and packing of axons, axonal caliber, membrane permeability, and presence of other cells such as glia, can also contribute to DTI changes in ordered axonal systems (Le Bihan et al. 2001; Le Bihan et al. 1993). Changes in cell body characteristics may contribute to DTI changes in less organized tissue, such as cortical regions. High anisotropic diffusion and low mean diffusivity or apparent diffusion coefficient have been observed in brain cystic lesions (Gupta et al. 2005), normal developing cortical brain regions (Miller et al. 2003), and epidermoid tumors (Koot et al. 2003).

Axial and radial diffusivity changes with age

Multiple brain regions showed negative correlations between axial and radial diffusivity values in combined male and female data and age. Since axial diffusivity measures diffusion of water parallel to tissue fibers, principally indicating axonal status (Song et al. 2002; Song et al. 2005), reduced axial diffusivity with age may result from increased numbers of brain fibers or increased axonal caliber in those areas allowing fibers to become less straight due to reduced inter-axonal space (Mukherjee et al. 2002; Qiu et al. 2008; Suzuki et al. 2003; Takahashi et al. 2000).

Since radial diffusivity measures diffusion of water perpendicular to fibers, values mainly reflect myelin changes (Song et al. 2002; Song et al. 2005). Reduction in radial diffusivity values with age may result from increased myelin development (Qiu et al. 2008; Suzuki et al. 2003), since thickening of myelin will reduce perpendicular water diffusion.

Myelin and axonal density, as well as axonal arborization, increase with age up to the third decade of life (Sowell et al. 2003; Toga et al. 2006). After the third decade, slow, natural degradation of fiber characteristics appears as aging proceeds (Hasan 2006).

Male-female differences

Several brain regions, including the putamen, amygdala, temporal white matter, and cerebellar peduncles showed increased axial diffusivity, and cingulate, ventral hippocampus, amygdala, midline occipital gray matter, thalamus and hypothalamus, and rostral cerebellar cortex showed increased radial diffusivity in females over males. The relative increase in axial or radial diffusivity values in females suggests reduced axonal density or caliber, and myelin, respectively, and cortical brain sites that showed increased axial or radial diffusivity values indicate less organization in those sites in females. In addition to slower global and regional gray and white matter development in females over males in pediatric subjects (Giedd et al. 1999), it appears that organization of those fibers with respect to the issues related to myelination and axonal development follows a different time course between sexes. Females show less-reduced axial and radial diffusivity at comparable ages over values for males, which, we speculate, may allow for more functional plasticity in females over males. We captured measures of axonal structure and organization at a time period before the maximal peak of axonal development, and demonstrate that major gender differences exist. Such delayed developmental trajectories in several brain sites, including the frontal lobe, cingulate, thalamus, and hypothalamus, are reflected also as reduced tissue changes in adult females over healthy adult males, as measured by voxel-based morphometry procedures (Takahashi et al. 2010). The findings here of differential gender-based myelination and axonal development in developing subjects may contribute to the well-described cognitive and emotional superiority in females over males in this age period (Kring and Gordon 1998; Mann et al. 1990).

Conclusions

Several brain sites showed inverse correlations between axial and radial diffusivity values and age, except for the right mid hippocampus, suggesting increased axonal density, caliber, and myelin with age. Male-female axial and radial diffusivity differences appeared in multiple brain areas within the rostral brain, thalamic and hypothalamic sites, as well as in cerebellar areas. These normal axial and radial diffusivity values, derived from several regions across the brain, give baseline values against which pathological tissue changes can be evaluated. The gender differences in fiber organization in several brain structures may significantly contribute to sex-related functions mediated by these structures. Normal age-related axial and radial diffusivity changes and gender differences in several brain areas make necessary a requirement for partitioning age- and gender-related changes during examination of pathology in these adolescent and young adult subjects.

Acknowledgments

The authors thank Ms. Rebecca Harper and Mr. Edwin M. Valladares for assistance with data collection.

Grant Support: This research was supported by the National Institute of Child Health and Human Development R01 HD-22695.

References

Ashburner J, Friston KJ. Unified segmentation. NeuroImage. 2005; 26(3):839–851. [PubMed: 15955494]

Barnea-Goraly N, Menon V, Eckert M, Tamm L, Bammer R, Karchemskiy A, Dant CC, Reiss AL. White matter development during childhood and adolescence: a cross-sectional diffusion tensor imaging study. Cereb Cortex. 2005; 15(12):1848–1854. [PubMed: 15758200]

Basser PJ, Pierpaoli C. A simplified method to measure the diffusion tensor from seven MR images. Magn Reson Med. 1998; 39(6):928–934. [PubMed: 9621916]

Della Nave R, Ginestroni A, Diciotti S, Salvatore E, Soricelli A, Mascalchi M. Axial diffusivity is increased in the degenerating superior cerebellar peduncles of Friedreich's ataxia. Neuroradiology. 2010; 53(5):367–372. [PubMed: 21128070]

DeLuca GC, Williams K, Evangelou N, Ebers GC, Esiri MM. The contribution of demyelination to axonal loss in multiple sclerosis. Brain. 2006; 129(Pt 6):1507–1516. [PubMed: 16597651]

Filippi M, Cercignani M, Inglese M, Horsfield MA, Comi G. Diffusion tensor magnetic resonance imaging in multiple sclerosis. Neurology. 2001; 56(3):304–311. [PubMed: 11171893]

Giedd JN, Blumenthal J, Jeffries NO, Castellanos FX, Liu H, Zijdenbos A, Paus T, Evans AC, Rapoport JL. Brain development during childhood and adolescence: a longitudinal MRI study. Nat Neurosci. 1999; 2(10):861–863. [PubMed: 10491603]

Guo AC, Petrella JR, Kurtzberg J, Provenzale JM. Evaluation of white matter anisotropy in Krabbe disease with diffusion tensor MR imaging: initial experience. Radiology. 2001; 218(3):809–815. [PubMed: 11230660]

Gupta RK, Hasan KM, Mishra AM, Jha D, Husain M, Prasad KN, Narayana PA. High fractional anisotropy in brain abscesses versus other cystic intracranial lesions. Am J Neuroradiol. 2005; 26(5):1107–1114. [PubMed: 15891168]

Hasan, KM. Fundamentals of diffusion tensor imaging of the entire human brain: review of basic theory, data acquisition, processing and potential applications at 1.5 T and 3.0 T. In: Chen, FJ., editor. Progress in brain mapping research. Hauppauge, New York, USA: Nova Science Publishers; 2006. p. 1-80.

Hasan KM, Eluvathingal TJ, Kramer LA, Ewing-Cobbs L, Dennis M, Fletcher JM. White matter microstructural abnormalities in children with spina bifida myelomeningocele and hydrocephalus: a diffusion tensor tractography study of the association pathways. J Magn Reson Imaging. 2008; 27(4):700–709. [PubMed: 18302204]

Huisman TA, Schwamm LH, Schaefer PW, Koroshetz WJ, Shetty-Alva N, Ozsunar Y, Wu O, Sorensen AG. Diffusion tensor imaging as potential biomarker of white matter injury in diffuse axonal injury. Am J Neuroradiol. 2004; 25(3):370–376. [PubMed: 15037457]

Jiang H, van Zijl PC, Kim J, Pearlson GD, Mori S. DtiStudio: resource program for diffusion tensor computation and fiber bundle tracking. Comput Methods Programs Biomed. 2006; 81(2):106–116. [PubMed: 16413083]

Jones K, Johnson KA, Becker JA, Spiers PA, Albert MS, Holman BL. Use of singular value decomposition to characterize age and gender differences in SPECT cerebral perfusion. J Nucl Med. 1998; 39(6):965–973. [PubMed: 9627327]

Koot RW, Jagtap AP, Akkerman EM, Den Heeten GJ, Majoie CB. Epidermoid of the lateral ventricle: evaluation with diffusion-weighted and diffusion tensor imaging. Clin Neurol Neurosurg. 2003; 105(4):270–273. [PubMed: 12954544]

Kring AM, Gordon AH. Sex differences in emotion: expression, experience, and physiology. J Pers Soc Psychol. 1998; 74(3):686–703. [PubMed: 9523412]

Kumar R, Delshad S, Macey PM, Woo MA, Harper RM. Development of T2-relaxation values in regional brain sites during adolescence. Magn Reson Imaging. 2011a; 29(2):185–193. [PubMed: 20933351]

Kumar R, Macey PM, Woo MA, Alger JR, Harper RM. Diffusion tensor imaging demonstrates brainstem and cerebellar abnormalities in congenital central hypoventilation syndrome. Pediatr Res. 2008; 64(3):275–280. [PubMed: 18458651]

Kumar R, Macey PM, Woo MA, Harper RM. Rostral brain axonal injury in congenital central hypoventilation syndrome. J Neurosci Res. 2010; 88(10):2146–2154. [PubMed: 20209631]

Kumar R, Woo MA, Macey PM, Fonarow GC, Hamilton MA, Harper RM. Brain axonal and myelin evaluation in heart failure. J Neurol Sci. 2011b

Larsson EM, Englund E, Sjobeck M, Latt J, Brockstedt S. MRI with diffusion tensor imaging post-mortem at 3.0 T in a patient with frontotemporal dementia. Dement Geriatr Cogn Disord. 2004; 17(4):316–319. [PubMed: 15178944]

Le Bihan D, Mangin JF, Poupon C, Clark CA, Pappata S, Molko N, Chabriat H. Diffusion tensor imaging: concepts and applications. J Magn Reson Imaging. 2001; 13(4):534–546. [PubMed: 11276097]

Le Bihan D, Turner R, Douek P. Is water diffusion restricted in human brain white matter? An echo-planar NMR imaging study. Neuroreport. 1993; 4(7):887–890. [PubMed: 8369479]

Mann VA, Sasanuma S, Sakuma N, Masaki S. Sex differences in cognitive abilities: a cross-cultural perspective. Neuropsychologia. 1990; 28(10):1063–1077. [PubMed: 2267058]

Miller JH, McKinstry RC, Philip JV, Mukherjee P, Neil JJ. Diffusion-tensor MR imaging of normal brain maturation: a guide to structural development and myelination. Am J Roentgenol. 2003; 180(3):851–859. [PubMed: 12591710]

Mitchell LA, Harvey AS, Coleman LT, Mandelstam SA, Jackson GD. Anterior temporal changes on MR images of children with hippocampal sclerosis: an effect of seizures on the immature brain? Am J Neuroradiol. 2003; 24(8):1670–1677. [PubMed: 13679290]

Mukherjee P, McKinstry RC. Diffusion tensor imaging and tractography of human brain development. Neuroimaging Clin N Am. 2006; 16(1):19–43. vii. [PubMed: 16543084]

Mukherjee P, Miller JH, Shimony JS, Philip JV, Nehra D, Snyder AZ, Conturo TE, Neil JJ, McKinstry RC. Diffusion-tensor MR imaging of gray and white matter development during normal human brain maturation. Am J Neuroradiol. 2002; 23(9):1445–1456. [PubMed: 12372731]

Neil JJ, Shiran SI, McKinstry RC, Schefft GL, Snyder AZ, Almli CR, Akbudak E, Aronovitz JA, Miller JP, Lee BC, Conturo TE. Normal brain in human newborns: apparent diffusion coefficient and diffusion anisotropy measured by using diffusion tensor MR imaging. Radiology. 1998; 209(1):57–66. [PubMed: 9769812]

Ogren JA, Macey PM, Kumar R, Woo MA, Harper RM. Central autonomic regulation in congenital central hypoventilation syndrome. Neuroscience. 2010; 167(4):1249–1256. [PubMed: 20211704]

Pierpaoli C, Basser PJ. Toward a quantitative assessment of diffusion anisotropy. Magn Reson Med. 1996; 36(6):893–906. [PubMed: 8946355]

Qiu D, Tan LH, Zhou K, Khong PL. Diffusion tensor imaging of normal white matter maturation from late childhood to young adulthood: voxel-wise evaluation of mean diffusivity, fractional anisotropy, radial and axial diffusivities, and correlation with reading development. NeuroImage. 2008; 41(2):223–232. [PubMed: 18395471]

Rorden C, Karnath HO, Bonilha L. Improving lesion-symptom mapping. J Cogn Neurosci. 2007; 19(7):1081–1088. [PubMed: 17583985]

Song SK, Sun SW, Ramsbottom MJ, Chang C, Russell J, Cross AH. Dysmyelination revealed through MRI as increased radial (but unchanged axial) diffusion of water. NeuroImage. 2002; 17(3):1429–1436. [PubMed: 12414282]

Song SK, Yoshino J, Le TQ, Lin SJ, Sun SW, Cross AH, Armstrong RC. Demyelination increases radial diffusivity in corpus callosum of mouse brain. NeuroImage. 2005; 26(1):132–140. [PubMed: 15862213]

Sowell ER, Peterson BS, Thompson PM, Welcome SE, Henkenius AL, Toga AW. Mapping cortical change across the human life span. Nat Neurosci. 2003; 6(3):309–315. [PubMed: 12548289]

Suzuki Y, Matsuzawa H, Kwee IL, Nakada T. Absolute eigenvalue diffusion tensor analysis for human brain maturation. NMR Biomed. 2003; 16(5):257–260. [PubMed: 14648885]

Takahashi M, Ono J, Harada K, Maeda M, Hackney DB. Diffusional anisotropy in cranial nerves with maturation: quantitative evaluation with diffusion MR imaging in rats. Radiology. 2000; 216(3): 881–885. [PubMed: 10966726]

Takahashi R, Ishii K, Kakigi T, Yokoyama K. Gender and age differences in normal adult human brain: Voxel-based morphometric study. Hum Brain Mapp. 2010

Toga AW, Thompson PM, Sowell ER. Mapping brain maturation. Trends Neurosci. 2006; 29(3):148–159. [PubMed: 16472876]

Trapp BD, Peterson J, Ransohoff RM, Rudick R, Mork S, Bo L. Axonal transection in the lesions of multiple sclerosis. N Engl J Med. 1998; 338(5):278–285. [PubMed: 9445407]

Werring DJ, Toosy AT, Clark CA, Parker GJ, Barker GJ, Miller DH, Thompson AJ. Diffusion tensor imaging can detect and quantify corticospinal tract degeneration after stroke. J Neurol Neurosurg Psychiatry. 2000; 69(2):269–272. [PubMed: 10896709]

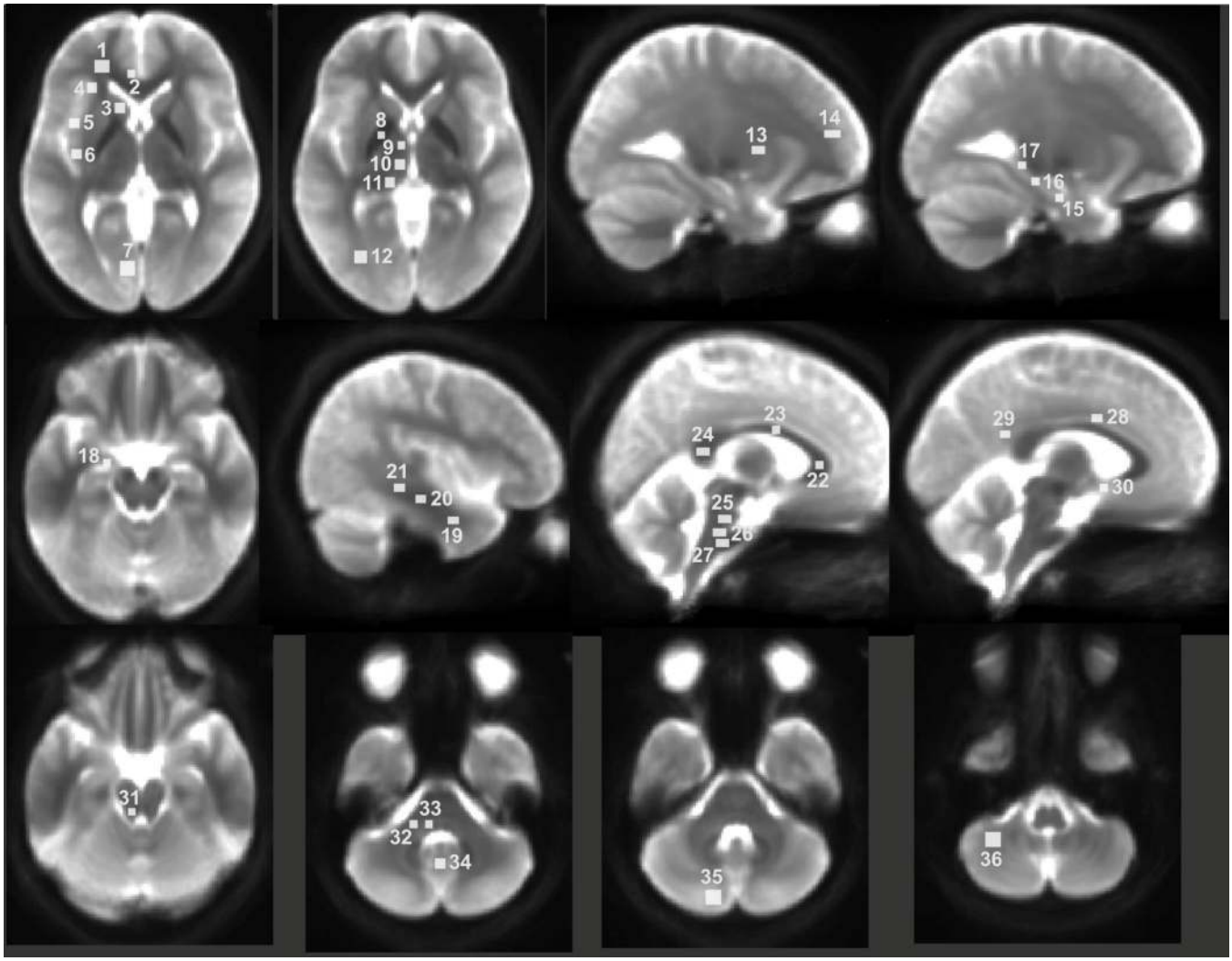

Fig. 1.

Mean background images, derived from normalized and averaged b0 images of all individuals, with regions-of-interest (ROIs). The rectangular ROIs were used to calculate regional axial and radial diffusivity values, which are shown only for the left side on background images for clarity. 1, frontal white matter; 2, anterior cingulate; 3, caudate nucleus; 4, anterior insula; 5, mid insula; 6, posterior insula; 7, midline occipital gray matter; 8, globus pallidus; 9, anterior thalamus; 10, mid thalamus; 11, posterior thalamus; 12, occipital white matter; 13, putamen; 14, frontal gray matter; 15, ventral hippocampus; 16, mid hippocampus; 17, dorsal hippocampus; 18, amygdala; 19, ventral temporal white matter; 20, mid temporal white matter; 21, dorsal temporal white matter; 22, anterior corpus callosum; 23, mid corpus callosum; 24, posterior corpus callosum; 25, caudal pons; 26, mid pons; 27, ventral pons; 28, mid cingulate; 29, posterior cingulate; 30, hypothalamus; 31, superior cerebellar peduncle; 32, mid cerebellar peduncle; 33, inferior cerebellar peduncle; 34 cerebellar deep nuclei; 35, caudal cerebellar cortex; 36, rostral cerebellar cortex.

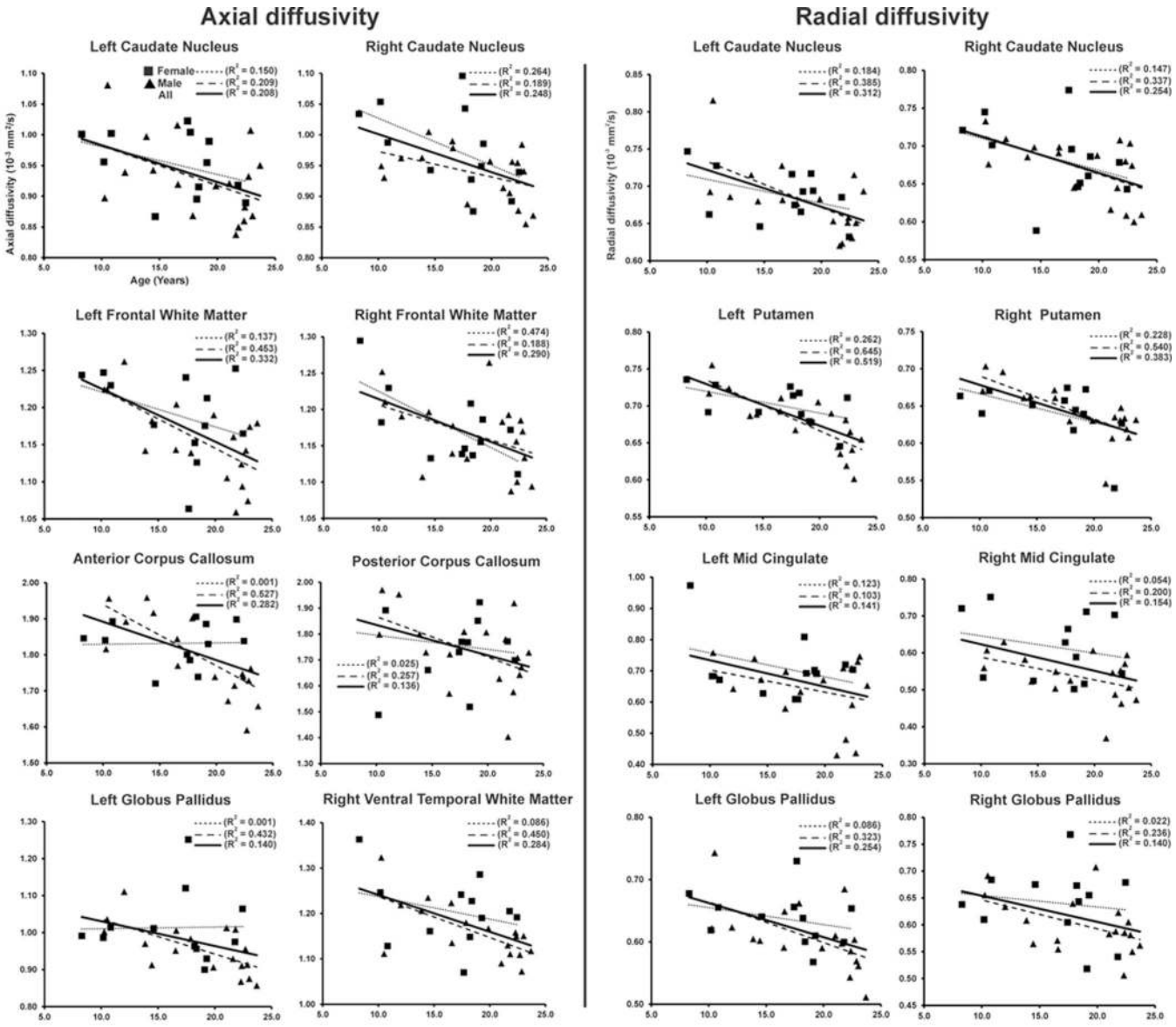

Fig. 2.

Correlations between combined, and separately, male, and female axial and radial diffusivity values, derived from multiple rostral brain sites, and age. Corresponding sold and dotted lines on the scatter plots display best fit lines for the combined, male, and female data.

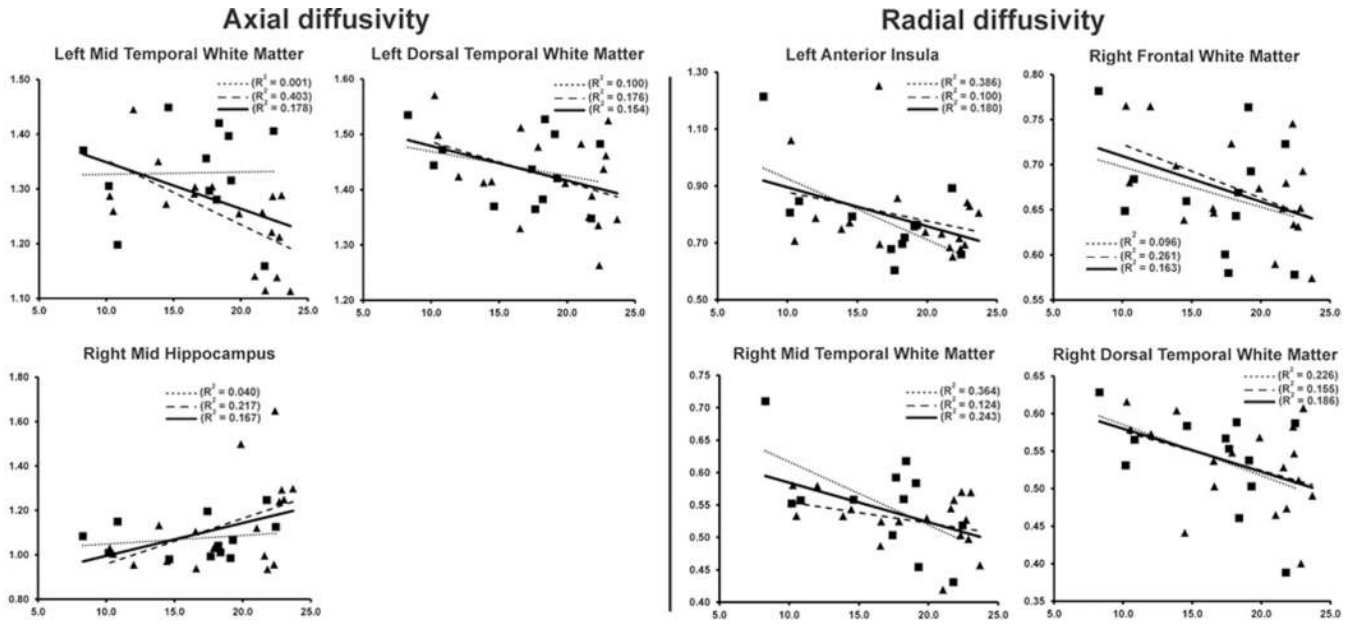

Fig. 3.

Rostral brain sites showing correlations between combined, male, and female axial and radial diffusivity values and age. Figure conventions are the same as in Fig. 2.

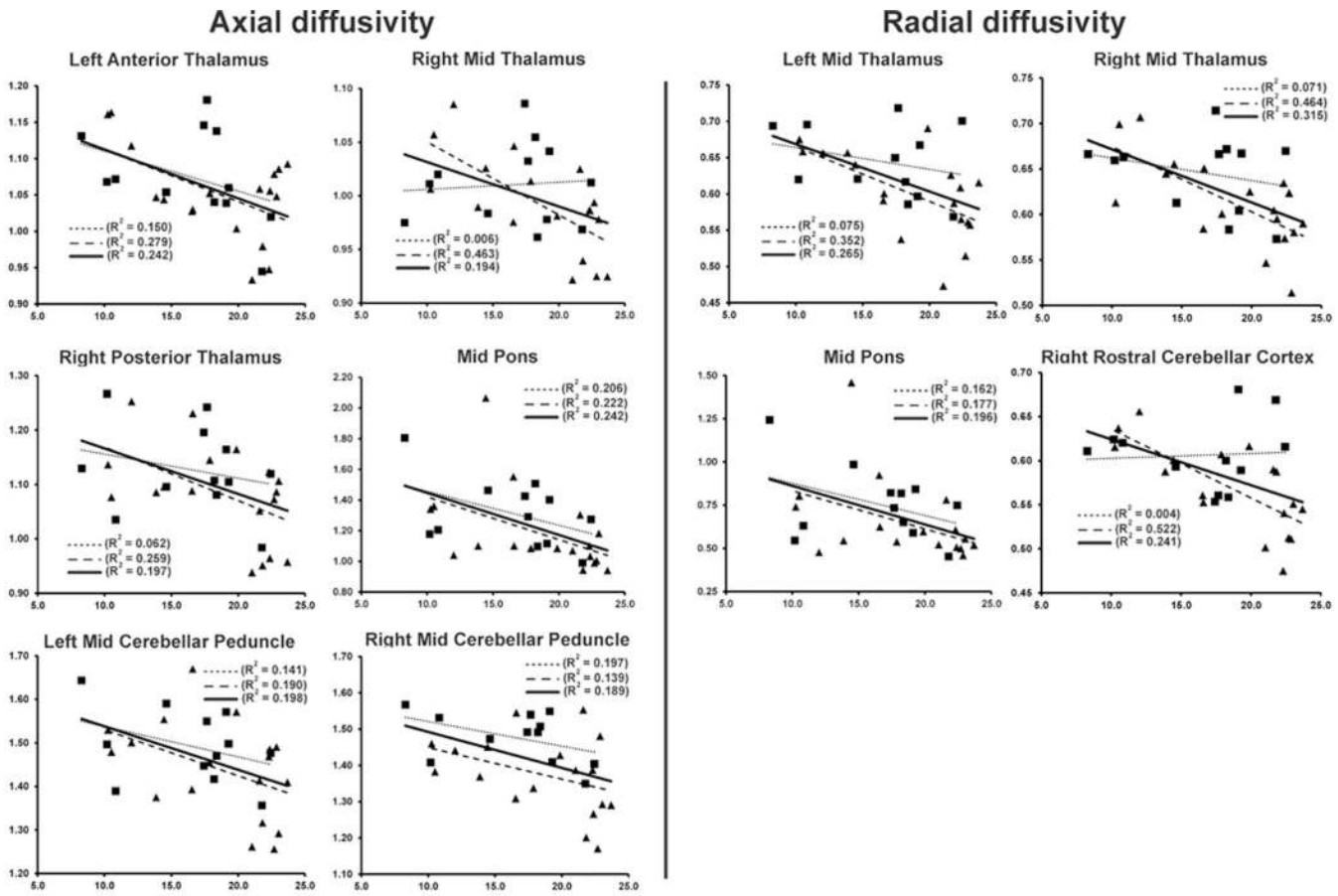

Fig. 4.

Thalamic, pontine, and cerebellar regions showing correlations between combined, male, and female, axial and radial diffusivity values and age. Figure conventions are the same as in Fig. 2.

J Neurosci Res. Author manuscript; available in PMC 2013 February 1.

Table 1

Axial and radial diffusivity values ($\times 10^{-3}$ mm^2/sec) of various sites within the rostral brain, and male-female differences.

Brain structures (ROI size, 12–243 mm^3)	**Axial diffusivity (n = 30)**	**Axial diffusivity (Male, 18)**	**Axial diffusivity (Female, 12)**	**Radial diffusivity (n = 30)**	**Radial diffusivity (Male, 18)**	**Radial diffusivity (Female, 12)**
L Amyg*†	1.12±0.16	1.06±0.16	1.20±0.12	0.82±0.11	0.78±0.10	0.87±0.09
R Amyg	1.10±0.14	1.08±0.12	1.14±0.17	0.81±0.10	0.80±0.08	0.83±0.13
L Ant Cing	1.18±0.07	1.19±0.07	1.16±0.06	0.71±0.08	0.70±0.08	0.73±0.07
R Ant Cing	1.19±0.13	1.18±0.11	1.21±0.16	0.76±0.12	0.73±0.12	0.80±0.13
L Mid Cing	1.27±0.10	1.27±0.10	1.28±0.10	0.67±0.10	0.64±0.10	0.71±0.10
R Mid Cing†	1.22±0.09	1.21±0.10	1.24±0.07	0.57±0.08	0.54±0.06	0.62±0.09
L Post Cing	1.09±0.07	1.08±0.05	1.11±0.08	0.73±0.07	0.73±0.06	0.74±0.09
R Post Cing	1.11±0.09	1.10±0.07	1.14±0.12	0.79±0.08	0.79±0.07	0.80±0.10
Ant Cor Call	1.81±0.09	1.80±0.11	1.83±0.06	0.30±0.07	0.31±0.08	0.28±0.05
Mid Cor Call	1.58±0.11	1.56±0.12	1.61±0.11	0.46±0.11	0.44±0.11	0.49±0.10
Post Cor Call	1.74±0.15	1.73±0.14	1.76±0.16	0.35±0.16	0.37±0.16	0.33±0.16
L Ant Insula	1.17±0.13	1.17±0.14	1.16±0.13	0.79±0.15	0.79±0.15	0.79±0.16
R Ant Insula	1.20±0.14	1.20±0.15	1.20±0.14	0.83±0.13	0.86±0.13	0.78±0.12
L Mid Insula	1.32±0.20	1.35±0.21	1.28±0.18	0.97±0.17	1.01±0.18	0.91±0.15
R Mid Insula	1.20±0.15	1.21±0.16	1.19±0.13	0.85±0.13	0.87±0.14	0.82±0.10
L Post Insula	1.09±0.07	1.08±0.08	1.09±0.05	0.72±0.05	0.72±0.06	0.71±0.03
R Post Insula	1.14±0.13	1.14±0.15	1.14±0.08	0.77±0.12	0.78±0.14	0.75±0.07
L Cau Nuclei	0.94±0.06	0.93±0.07	0.95±0.05	0.68±0.04	0.68±0.05	0.69±0.03
R Cau Nuclei	0.95±0.06	0.94±0.04	0.98±0.07	0.68±0.04	0.67±0.04	0.68±0.05
L Fron Gray Matt	1.14±0.06	1.13±0.06	1.16±0.07	0.70±0.11	0.71±0.12	0.70±0.12
R Fron Gray Matt	1.12±0.07	1.11±0.07	1.14±0.07	0.71±0.09	0.71±0.09	0.72±0.10
L Fron White Matt	1.17±0.06	1.16±0.05	1.19±0.06	0.67±0.06	0.67±0.05	0.67±0.07
R Fron White Matt	1.17±0.05	1.17±0.05	1.17±0.05	0.67±0.06	0.67±0.05	0.67±0.07
L Globus Pallidus	0.98±0.08	0.96±0.07	1.01±0.95	0.62±0.05	0.61±0.05	0.64±0.04
R Globus Pallidus	0.98±0.09	0.96±0.07	1.01±0.10	0.62±0.06	0.60±0.05	0.64±0.07

Brain structures (ROI size, 12–243 mm^3)	Axial diffusivity (n = 30)	Axial diffusivity (Male, 18)	Axial diffusivity (Female, 12)	Radial diffusivity (n = 30)	Radial diffusivity (Male, 18)	Radial diffusivity (Female, 12)
L Putamen*	0.90±0.04	0.88±0.03	0.93±0.04	0.69±0.04	0.68±0.04	0.70±0.03
R Putamen	0.86±0.05	0.85±0.04	0.88±0.07	0.64±0.04	0.64±0.04	0.64±0.04
L Ven Hipp†	1.10±0.11	1.08±0.12	1.14±0.09	0.84±0.08	0.81±0.08	0.88±0.07
R Ven Hipp	1.05±0.09	1.05±0.09	1.04±0.09	0.77±0.07	0.77±0.08	0.77±0.07
L Mid Hipp	1.17±0.17	1.15±0.17	1.20±0.17	0.81±0.10	0.80±0.10	0.83±0.11
R Mid Hipp	1.11±0.17	1.13±0.20	1.07±0.09	0.81±0.11	0.83±0.13	0.78±0.07
L Dor Hipp	1.48±0.16	1.45±0.17	1.51±0.16	0.74±0.09	0.72±0.08	0.78±0.09
R Dor Hipp	1.39±0.18	1.39±0.18	1.39±0.19	0.82±0.10	0.82±0.11	0.81±0.09
L Ven Tem White Matt	1.23±0.06	1.23±0.07	1.24±0.06	0.64±0.05	0.64±0.06	0.63±0.03
R Ven Tem White Matt	1.18±0.07	1.16±0.06	1.20±0.08	0.61±0.06	0.60±0.08	0.62±0.04
L Mid Tem White Matt*	1.28±0.09	1.25±0.09	1.33±0.09	0.50±0.06	0.50±0.06	0.50±0.06
R Mid Tem White Matt	1.32±0.09	1.32±0.06	1.34±0.12	0.53±0.06	0.53±0.04	0.55±0.07
L Dor Tem White Matt	1.43±0.07	1.42±0.08	1.44±0.06	0.51±0.06	0.50±0.07	0.52±0.05
R Dor Tem White Matt	1.44±0.08	1.43±0.08	1.45±0.09	0.54±0.06	0.53±0.06	0.54±0.07
L Midl Occ Gray Matt	1.15±0.09	1.15±0.09	1.15±0.09	0.80±0.09	0.83±0.10	0.77±0.08
R Midl Occ Gray Matt†	1.16±0.14	1.11±0.08	1.23±0.19	0.80±0.11	0.77±0.09	0.85±0.12
L Occ White Matt	1.17±0.17	1.15±0.17	1.20±0.17	0.57±0.04	0.58±0.05	0.57±0.03
R Occ White Matt	1.25±0.09	1.27±0.08	1.23±0.09	0.57±0.05	0.56±0.05	0.58±0.04

Table legend: L = Left; R = Right; Amyg = Amygdala; Ant = Anterior; Cing = Cingulate; Mid = Middle; Post = Posterior; Cor Call = Corpus Callosum; Cau = Caudate; Fron = Frontal; Matt = Matter; Ven = Ventral; Hipp = Hippocampus; Dor = Dorsal; Tem = Temporal; Midl = Midline.

*Significant differences in axial diffusivity values between males and females ($p < 0.05$).

†Significant differences in radial diffusivity values between males and females ($p < 0.05$).

J Neurosci Res. Author manuscript; available in PMC 2013 February 1.

Table 2

Axial and radial diffusivity values ($\times 10^{-3}$ mm^2/sec) of brain regions within the thalamus and hypothalamus, and male female differences.

Brain structures (ROI size, 12–75 mm^3)	Axial diffusivity (n = 30)	Axial diffusivity (Male, 18)	Axial diffusivity (Female, 12)	Radial diffusivity (n = 30)	Radial diffusivity (Male, 18)	Radial diffusivity (Female, 12)
L Ant Thal	1.06±0.06	1.05±0.06	1.07±0.07	0.60±0.06	0.59±0.05	0.62±0.06
R Ant Thal	1.05±0.06	1.04±0.06	1.06±0.06	0.61±0.06	0.59±0.05	0.64±0.06
L Mid Thal†	0.98±0.05	0.97±0.05	1.00±0.05	0.62±0.06	0.60±0.06	0.64±0.05
R Mid Thal	0.10±0.04	0.99±0.05	1.01±0.04	0.63±0.05	0.61±0.05	0.65±0.04
L Post Thal	1.03±0.11	1.02±0.12	1.04±0.09	0.60±0.07	0.62±0.09	0.58±0.04
R Post Thal	1.10±0.09	1.08±0.09	1.13±0.08	0.62±0.06	0.62±0.07	0.62±0.04
L Hypothal	1.06±0.07	1.04±0.06	1.08±0.09	0.76±0.06	0.75±0.05	0.79±0.08
R Hypothal†	1.05±0.05	1.03±0.04	1.07±0.07	0.77±0.05	0.75±0.04	0.80±0.06

Table legend: L = Left; R = Right; Ant = Anterior; Thal = Thalamus; Mid = Middle; Post = Posterior; Hypothal = Hypothalamus.

*Significant differences in axial diffusivity values between males and females ($p < 0.05$).

†Significant differences in radial diffusivity values between males and females ($p < 0.05$).

J Neurosci Res. Author manuscript; available in PMC 2013 February 1.

Table 3

Axial and radial diffusivity values ($\times 10^{-3}$ mm^2/sec) of brain sites within the cerebellum and pons, and male-female differences in those areas.

Brain structures (ROI size, 27–147 mm^3)	Axial diffusivity (n = 30)	Axial diffusivity (Male, 18)	Axial diffusivity (Female, 12)	Radial diffusivity (n = 30)	Radial diffusivity (Male, 18)	Radial diffusivity (Female, 12)
Sup Pons	1.27±0.25	1.23±0.26	1.32±0.24	0.67±0.23	0.65±0.24	0.69±0.22
Mid Pons	1.23±0.26	1.18±0.27	1.31±0.22	0.69±0.23	0.64±0.24	0.75±0.21
Inf Pons	1.17±0.17	1.14±0.18	1.21±0.14	0.63±0.15	0.61±0.17	0.67±0.11
L Cau Cere Cor	1.02±0.09	1.03±0.09	1.01±0.10	0.73±0.08	0.74±0.08	0.72±0.08
R Cau Cere Cor	1.03±0.11	1.04±0.12	1.01±0.11	0.72±0.11	0.73±0.13	0.71±0.09
L Ros Cere Cor	0.94±0.05	0.94±0.04	0.95±0.06	0.59±0.05	0.59±0.05	0.59±0.06
R Ros Cere Cor†	0.91±0.05	0.90±0.05	0.93±0.05	0.58±0.05	0.57±0.05	0.61±0.04
Cere Deep Nuclei	0.10±0.07	1.00±0.08	0.99±0.03	0.62±0.04	0.62±0.05	0.62±0.03
L Inf Cere Ped	1.23±0.07	1.24±0.07	1.22±0.07	0.66±0.08	0.68±0.08	0.64±0.07
R Inf Cere Ped	1.42±0.14	1.40±0.13	1.46±0.16	0.58±0.16	0.54±0.14	0.64±0.17
L Mid Cere Ped	1.46±0.10	1.44±0.11	1.49±0.09	0.33±0.07	0.33±0.07	0.34±0.07
R Mid Cere Ped*	1.42±0.11	1.37±0.11	1.48±0.07	0.36±0.05	0.37±0.05	0.35±0.05
L Sup Cere Ped	1.43±0.06	1.43±0.07	1.43±0.04	0.34±0.06	0.33±0.06	0.36±0.05
R Sup Cere Ped	1.42±0.07	1.41±0.08	1.42±0.06	0.36±0.04	0.35±0.05	0.37±0.03

Table legend: Sup = Superior; Mid = Middle; Inf = Inferior; L = Left; R = Right; Cau = Caudal; Cere = Cerebellar; Cor = Cortex; Ped = Peduncle.

*Significant differences in axial diffusivity values between males and females ($p < 0.05$).

†Significant differences in radial diffusivity values between males and females ($p < 0.05$).